CrossMark

Equatorial Indian Ocean subsurface current variability in an Ocean General Circulation Model

C. Gnanaseelan[1] · Aditi Deshpande[1,2]

Abstract The variability of subsurface currents in the equatorial Indian Ocean is studied using high resolution Ocean General Circulation Model (OGCM) simulations during 1958–2009. February–March eastward equatorial subsurface current (ESC) shows weak variability whereas strong variability is observed in northern summer and fall ESC. An eastward subsurface current with maximum amplitude in the pycnocline is prominent right from summer to winter during strong Indian Ocean Dipole (IOD) years when air-sea coupling is significant. On the other hand during weak IOD years, both the air-sea coupling and the ESC are weak. This strongly suggests the role of ESC on the strength of IOD. The extension of the ESC to the summer months during the strong IOD years strengthens the oceanic response and supports intensification and maintenance of IODs through modulation of air sea coupling. Although the ESC is triggered by equatorial winds, the coupled air-sea interaction associated with IODs strengthens the ESC to persist for several seasons thereby establishing a positive feedback cycle with the surface. This suggests that the ESC plays a significant role in the coupled processes associated with the evolution and intensification of IOD events by cooling the eastern basin and strengthening thermocline-SST (sea surface temperature) interaction. As the impact of IOD events on Indian summer monsoon is significant only during strong IOD years, understanding and monitoring the evolution of ESC during these years is important for summer monsoon forecasting purposes. There is a westward phase propagation of anomalous subsurface currents which persists for a year during strong IOD years, whereas such persistence or phase propagation is not seen during weak IOD years, supporting the close association between ESC and strength of air sea coupling during strong IOD years. In this study we report the processes which strengthen the IOD events and the air sea coupling associated with IOD. It also unravels the connection between equatorial Indian Ocean circulation and evolution and strengthening of IOD.

1 Introduction

Equatorial Indian Ocean (EIO) subsurface is as dynamic and enigmatic as the surface. Over the equatorial Atlantic and Pacific Oceans, the prevailing trade winds drive a quasi permanent eastward zonal pressure gradient force along the equator leading to a quasi permanent eastward equatorial undercurrent (EUC) in both these oceans at a depth where surface wind stress driven current does not balance with the pressure gradient driven flow (e.g. Izumo 2005). The Indian Ocean EUC is a transient wave driven phenomenon, which occurs regularly during February–April and is modulated by the seasonal variations in circulation (Schott and McCreary 2001). Chen et al. (2015) showed strengthening and eastward extension of EUC during February to March before weakening in April–May by the high subsurface pressure in the eastern basin forced by the equatorial westerly winds. Iskandar et al. (2009) showed that the onset of westerly winds in spring and the induced spring Wyrtki jet (Wyrtki 1973) terminate the eastward pressure gradient force, which in turn reverses the eastward current in the

✉ C. Gnanaseelan
   seelan@tropmet.res.in

1   Indian Institute of Tropical Meteorology, Pune 411008, India

2   Savitribai Phule Pune University, Pune 411007, India

thermocline. Similarly, the fall Wyrtki jet also contributes to the termination of eastward pressure gradient force generated in summer. The interannual variability in the subsurface zonal current is as strong as the surface currents and therefore needs careful scrutiny.

Reppin et al. (1999) reported the occurrence of EUC from February to May of 1994 between 50 and 150 m, which disappeared in June but reappeared in August at a shallower depth with less transport. They attributed it to the El Niño forcing from the Pacific. It is important to mention here that during the monsoon transition periods (i.e. during April–May and October–November), the subsurface eastward current merges with the surface Wyrtki jets, whereas during the summer monsoon, the eastward current is weak in the subsurface. An anomalous summer eastward subsurface current is reported by Thompson et al. (2006) during positive Indian Ocean Dipole (IOD, Saji et al. 1999; Webster et al. 1999; Vinayachandran et al. 1999) years using model simulations. IOD is associated with strong easterly wind anomalies, which often weaken or reverse the surface currents, and therefore the Wyrtki jets are weaker than normal during these years (Gnanaseelan et al. 2012). The EUC is an important feature in the oceanic circulation, and is particularly important in the Indian Ocean region, because of its transient nature, as it maintains the mass and heat balance in the thermocline region. Recent studies have shown that IOD induced variability strongly governs the interannual variability in the subsurface currents (e.g. Thompson et al. 2006; Iskandar et al. 2009) though both IOD and El Niño governs the subsurface temperature variability (Sayantani and Gnanaseelan 2015). For this reason, the development of anomalous subsurface currents in the pycnocline or thermocline during IOD years and its role on the evolution of strong IOD events are emphasized in this study. The present study deals with the evolution and variability of the equatorial subsurface currents and its impact on the evolution and strength of IOD and the regional climate.

2 Model details, datasets and methodology used

The model used in the study is an Ocean General Circulation Model (OGCM) Modular Ocean Model (MOM4p1) set up over the Indo Pacific region (30°E–70°W, 60°S–30°N) with a uniform resolution of 0.25° × 0.25°. The model has 50 vertical levels with 10 m resolution in the upper 220 m and gradually increases up to 370 m in the deepest layer. The model is initialized using WOA2009 climatology and spun up for 100 years using CORE v2 (Griffies et al. 2009) Normal year forcing. The model is then integrated from 1958 to 2009 by forcing with CORE v2 Interannual Forcing. A detailed description of the model is given in Griffies et al. (2009) and Rahul and Gnanaseelan (2016). Empirical

orthogonal function (EOF) analysis and composite analysis are used for studying the subsurface current variability. The interannual anomalies are computed by subtracting the monthly mean climatology (computed for a 52 year period) from the respective monthly means of temperature, current etc. For EOF and composite analysis, the data has been regridded to 0.5° × 0.5° resolution. Monthly mean currents of Acoustic Doppler Current Profiler (ADCP) (McPhaden et al. 2009) mooring and Simple Ocean Data Assimilation (SODA) (Carton and Giese 2008) are used to validate the model subsurface zonal currents.

3 Equatorial Indian Ocean subsurface current and its variability

Figure 1 shows the comparison of monthly means of model zonal currents (shaded) at 90°E and 80.5°E at the equator with ADCP mooring currents (contours) at the same location. The model captures the annual cycle of both surface and subsurface currents very well. The vertical extent of Wyrtki jets is seen up to 80 m in both spring and fall, beyond which the currents weaken rapidly and reverse in the thermocline or pycnocline. The current literature does not have a consistent definition of Equatorial Undercurrent (EUC) for the Indian Ocean unlike in the Pacific (e.g. Izumo 2005) due to its transient nature. Different depth ranges are adopted in the observation based studies (e.g. Iskandar et al. (2009) reported EUC at 90–170 m and Reppin et al. (1999) reported EUC at 50–150 m) and model based studies (e.g. Swapna and Krishnan 2008) reported EUC at 100–150 m). Considering the variability in EUC depth range and to capture the EUC more cleanly, the average subsurface current between the isopycnals σ-23 and σ-25 is referred to as the equatorial subsurface current (ESC) or EUC or pycnocline current or subsurface current in the study. An eastward well defined ESC is evident during February and March. A significant interannual variability is evident in the subsurface zonal currents (Fig. 1). A well defined ESC is evident from August 2006 (an IOD year) to April 2007 also at both the buoy locations (Fig. 1). It is also important to record the differences in the intensity and extent (both depth and time) at the two buoy locations with significant interannual variability both at surface and subsurface currents. The westward phase propagation of both surface and subsurface currents is also evident in Fig. 1 and this propagation is much more convincing in Fig. 2. The westward phase propagation is due to the westward phase propagation in winds. Figure 2 also provides a comparison of model currents with both ADCP observations and SODA reanalysis. This further adds confidence to the model simulations. It is also important to note from Fig. 2 that the buoy at 80.5°E recorded higher magnitude
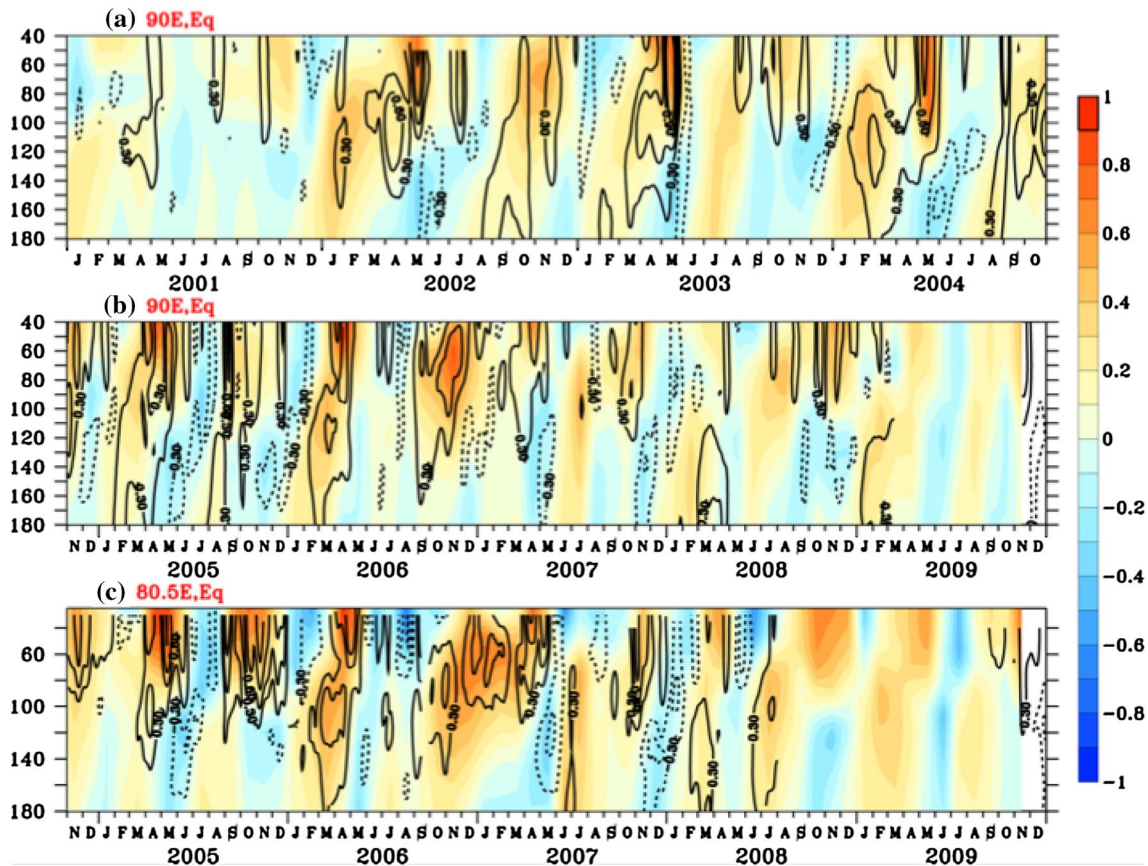
Fig. 1 Zonal currents from model (*shaded*) and ADCP moorings (*contours*) at **a, b** 90°E, equator and **c** 80.5°E, equator

of surface currents than that of 90°E in both the model and reanalysis, which are consistent with the observations. However the features are contrasting in the subsurface with stronger ESC at 90°E. This subsurface intensification is consistent with the surface weakening as both weakening of eastward surface jet and subsurface currents are primarily forced by anomalous easterly winds. Detailed analysis with the model simulation reveals that ESC in EIO is evident during all the IOD years right from the beginning of summer season. Since the ESC and its variability are well captured by the model and SODA, we used the model and SODA currents for detailed analysis. Figure 3 shows the climatological area averaged zonal currents over the equatorial region (60°E–90°E, 1.5°S–1.5°N) in the model (shaded) and SODA (contours). The annual cycle in both model and SODA shows the seasonal reversal of surface and subsurface currents. The climatological area averaged equatorial Indian Ocean zonal current shows that an ESC exists during the months of February to April and August to October in the thermocline or pycnocline. This ESC during February to April is wider, reaching up to 200 m, whereas the ESC during August to October is confined to a shallow (signals confined to 140 m) and narrow region.

The ESC in model and reanalysis are consistent with the observations.

The surface currents reverse four times in a year, flowing eastward during monsoon transition periods (boreal spring and fall), whereas westward current is evident during summer and winter monsoon period. During the monsoon transition periods, deep eastward surface currents are observed and are called Wyrtki jets, while the westward surface currents during monsoon periods are weaker and shallow. A canonical eastward ESC is seen in the Indian Ocean only during February–March. Figure 3 however reports a secondary eastward ESC during August to October.

4 Interannual variability of the subsurface current

The interannual variability of ESC is investigated using composite analysis of zonal current anomalies from both model and SODA (Fig. 4). The eastward undercurrent is well defined throughout the calendar year during positive IOD years (Fig. 4c). On the other hand during pure El Niño years (1965, 1986, 1987, 2002, 2004), the ESC weakens
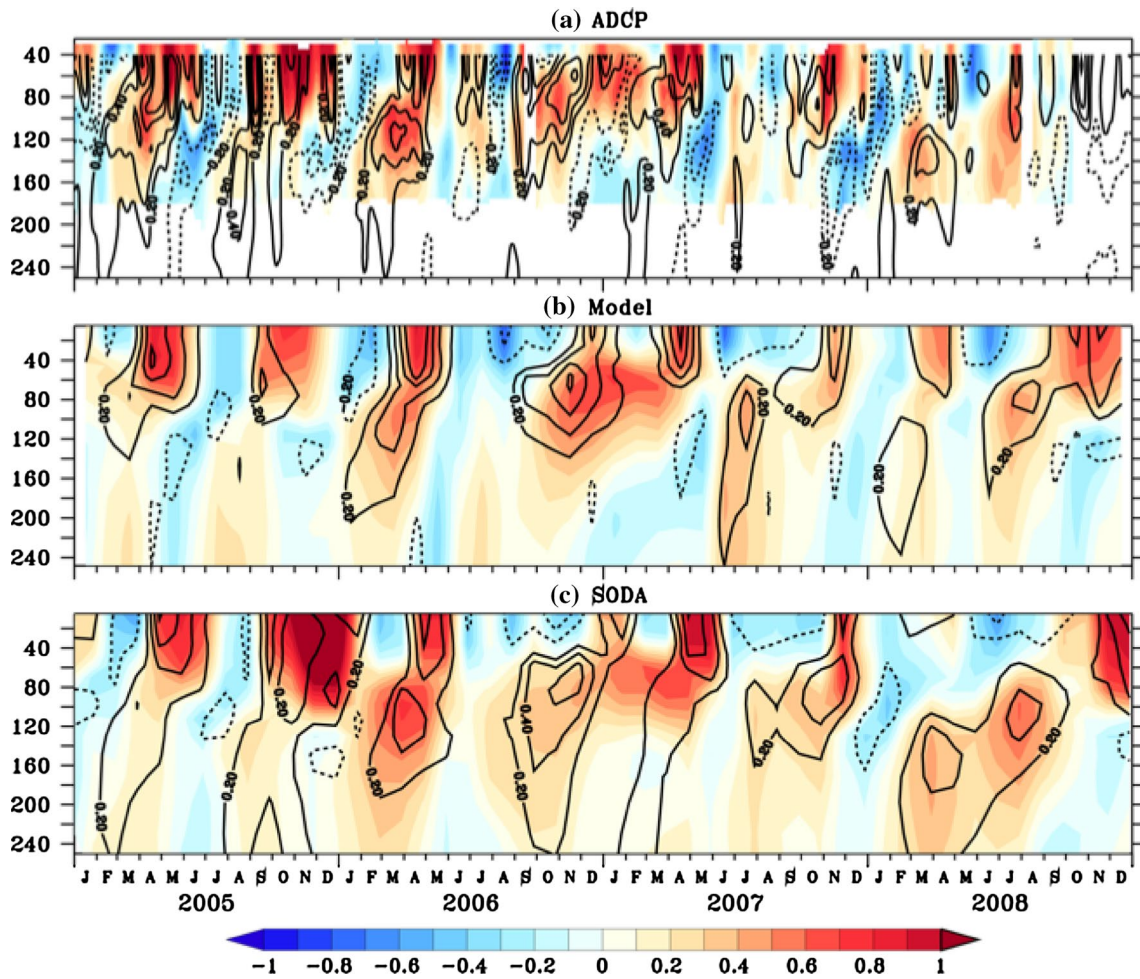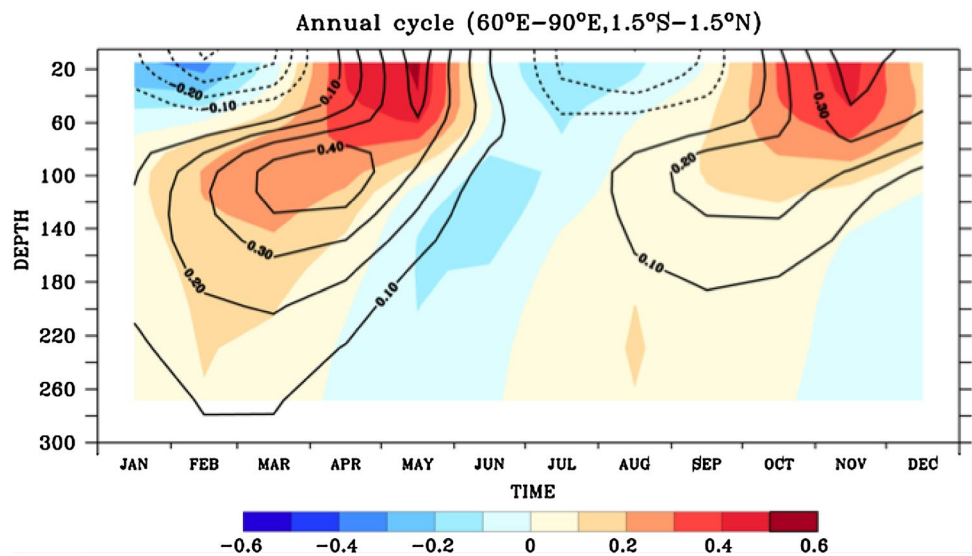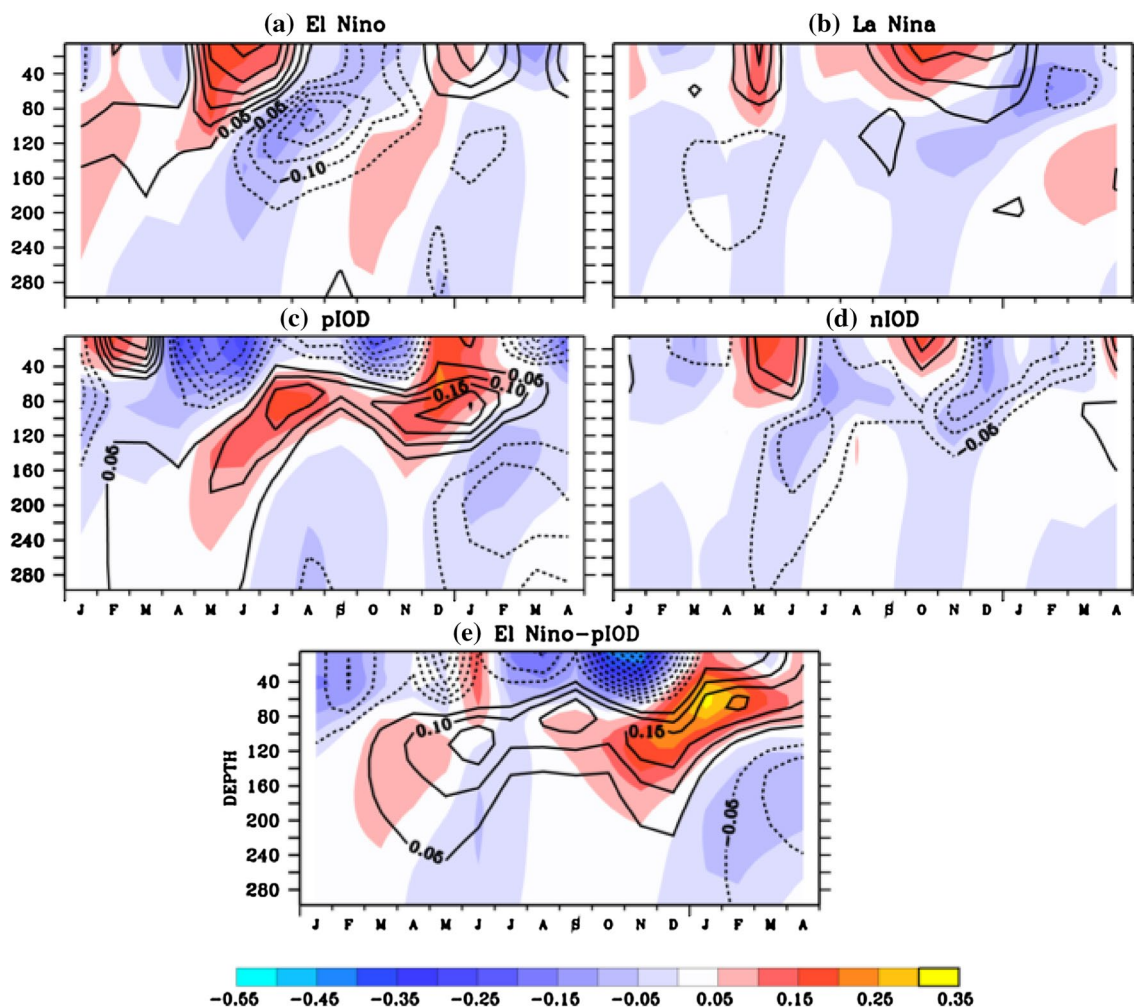
Fig. 2 Annual cycle of zonal current from 2005 to 2008 at 80.5°E (*shaded*) and 90°E (*contours*) from **a** ADCP, **b** model and **c** SODA

Fig. 3 Annual cycle (averaged during 1958–2008) of zonal current averaged over 60°E–90°E, 1.5°S–1.5°N from model (*shaded*) and SODA (*contours*)

Fig. 4 Composite evolution of area averaged (60°E–90°E, 1.5°S–1.5°N) zonal current anomalies for years of **a** El Niño years, **b** La Nina years, **c** p-IOD years, **d** n-IOD years and **e** El Niño–pIOD co-occurrence years from model (*shaded*) and SODA (*contours*)

during the summer monsoon period (anomalous westward subsurface currents). A similar weakening of ESC (anomalous westward subsurface currents) is seen during negative IOD years as well (Fig. 4d). In the case of La Niña years, no significant anomalies are observed in the subsurface zonal currents. The model composites (Fig. 4) are consistent with the SODA composites. From the above discussions it is evident that very strong quasi permanent features of ESC exist in the Indian Ocean during positive IOD years, especially during summer monsoon and fall season. The strongest variability in the ESC is evident during summer and fall seasons. These are consistent with Nyadjro and McPhaden (2014) and Zhang et al. (2014). Some of the noteworthy features are (1) strengthening (weakening) of spring (fall) Wyrtki jets during El Niño years, (2) weakening of both spring and fall Wyrtki jets during positive IOD years, (3) strengthening of summer ESC during positive IOD years with the strengthening of February to April ESC during the

following years, (4) weakening of February to April ESC during the years following negative IOD.

The interannual variability in the subsurface zonal currents is further investigated using EOF analysis of equatorial zonal current anomalies averaged over the isopycnal surfaces σ-23 and σ-25 (Fig. 5). The first mode of variability is found to be closely associated with IOD, with a significant correlation with dipole mode index (DMI). The EOFs of anomalous surface currents and wind stress are also shown in Fig. 5a, b for completeness, which are consistent with the surface variability reported in Gnanaseelan et al. (2012). The surface currents peak about 10° west of surface wind peak, whereas ESC shows double peak pattern with the peaks in both west and east of surface current peak. The time series analysis of the first principal component (PC-1) reveals that though the evolution of the ESC is unique in each of the anomalous years, there are certain years with anomalously strong eastward
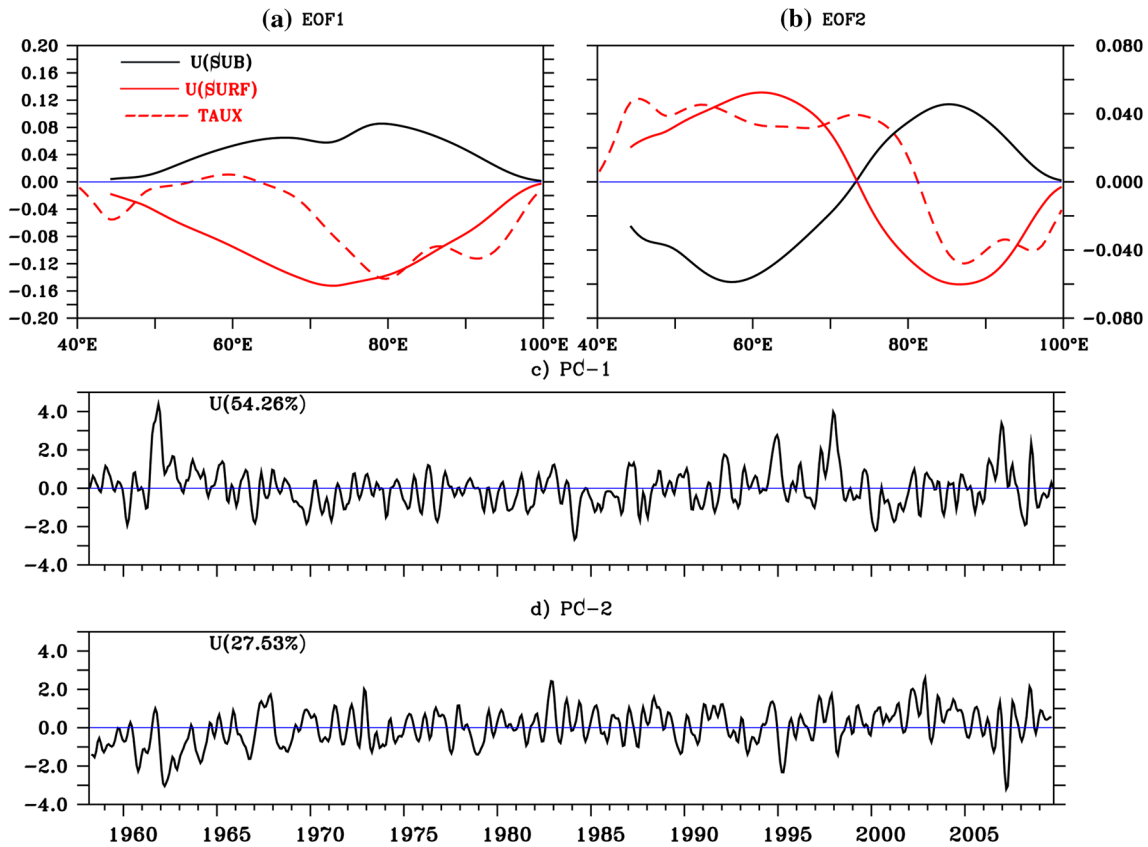
Fig. 5 a First EOF (EOF1) of subsurface zonal current anomalies (*black*), surface (15 m depth) zonal current anomalies (*red, thick*) and zonal windstress (*red, dash*) along the equator and **c** Principal compo-
nent (PC-1) of subsurface current anomalies. **b, d** Are same as **a, c**, but they correspond to second EOF (EOF2)

flowing ESC which extends through the summer monsoon season, and is found to be consistent with SODA. A detailed analysis of PC-1 reveals that the subsurface current variability is strongly associated with IOD, but not all IOD years show similar response. Swapna and Krishnan (2008) attributed this to strong monsoon forcing and its interaction with IOD. Some IOD years such as 1961, 1994, 1997, 2006 have strong response which persists for a longer period during the calendar year (Fig. 5c). On the other hand, years such as 1967, 1972, 1977 and 1982 have relatively subdued response even though the ESC is present during summer monsoon months. These years are found to be consistent with the strength of IOD as classified by Deshpande et al. (2014). They classified the years as strong and weak IOD years based on the differences in the air sea coupling strength during these years. The DMI, normalised D20 anomalies averaged over the eastern EIO region (D20 index), and normalised zonal wind anomalies similar to the index used by Gadgil et al. (2004) averaged over the equatorial region, 60°E–90°E, 2°S–2°N (wind index) and a combined index based on the above three indices (Deshpande et al. 2014) are used to classify strong and

weak IOD events. While DMI characterizes the anomalous SST behaviour over tropical Indian Ocean, the D20 index characterizes the strength of upwelling over the eastern EIO and the wind index is a measure of the atmospheric response of the coupled interaction associated with IOD. An IOD year is classified as a strong year when each of the three indices DMI, D20 index and wind index exceed one standard deviation during September–November (SON), and the combined index exceeds two-standard deviation. When the above three indices are within the range of half to one standard deviation, and the combined index is between one to two standard deviation during SON, the year is classified as a weak IOD year (Deshpande et al. 2014). List of strong and weak IOD years is given in Table 1.

Table 1 List of strong and weak IOD years as in Deshpande et al. (2014)

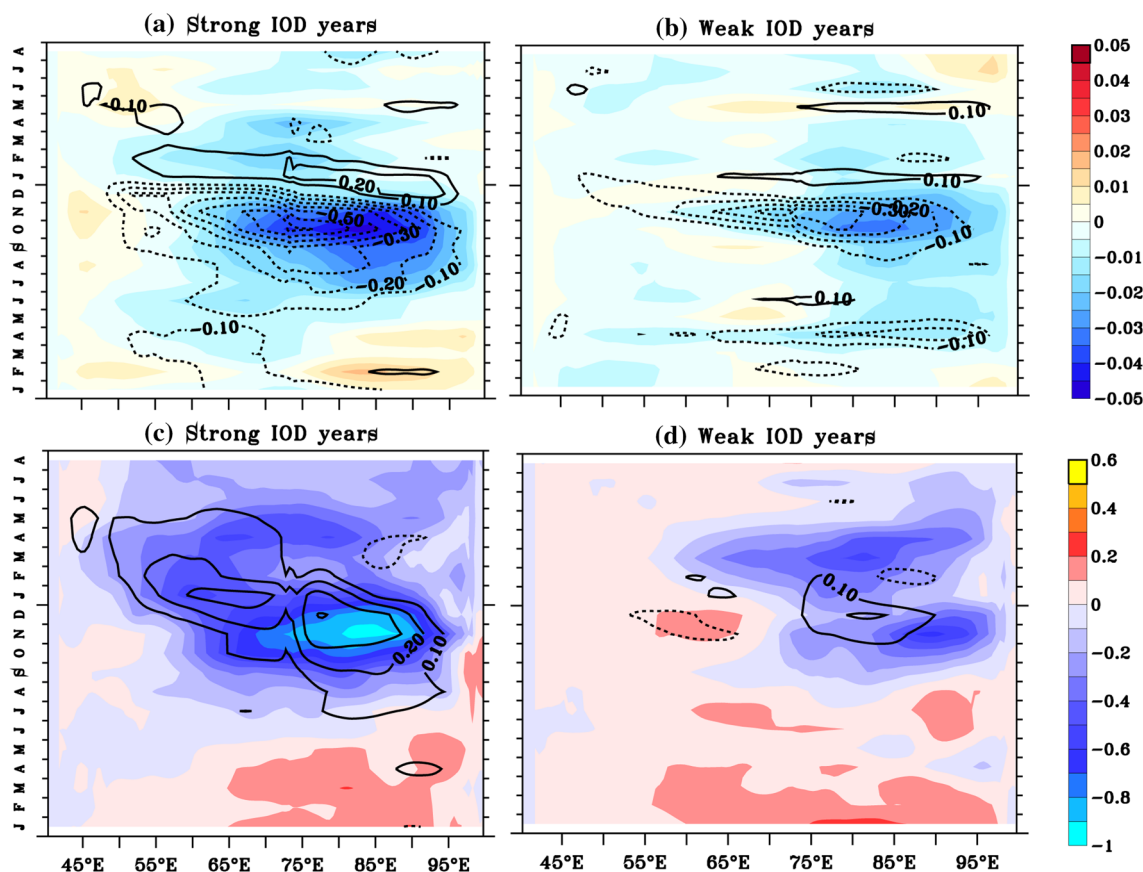| Strong IOD years	Weak IOD years
1961, 1994, 1997[a], 2006[a]	1963, 1967, 1972[a], 1977, 1982[a]

[a] El Niño-IOD co-occurrence years

The detailed analysis reveals the possible association between the summer and fall ESC with the air sea coupling strength of IOD. The second principal component (PC-2) has no significant correlation with either DMI or Niño 3.4 index (Fig. 5d) and may represent the variability associated with the internal variations of the system. The present study however is focused on the interannual variability of ESC associated with IOD and El Niño; hence the discussion on the internal dynamics is beyond the scope of this paper.

Figure 6 demonstrates the evolution of surface winds, currents, salinity in association with the evolution of subsurface currents during strong and weak IOD years. There is contrast in the evolution of surface winds, currents, salinity and subsurface currents during the strong and weak years. From the co-evolution of ESC and surface salinity, it is clearly evident that the subsurface current plays an important role in the thermocline-SST coupling leading to stronger IODs and stronger air sea coupling. The eastward subsurface currents and subsequent upwelling in the east support westward propagation of surface freshwater and

freshening of the central and western EIO. This freshening supports stronger air sea interaction and rainfall (Xie et al. 2002; Chowdary et al. 2009). All these are favourable for surface warming in the western region. This further assists convection over the western region and drive easterly wind anomalies. These are evident in the negative sea surface salinity and equatorial zonal wind anomalies. There is a westward phase propagation of anomalous subsurface currents which persists for a year during strong IOD years, whereas such persistence or phase propagation is not seen during weak IOD years. These anomalous subsurface currents are therefore closely associated with coupled processes during strong IOD years. It is important to note that the evolution of subsurface zonal current anomalies in the model is consistent with SODA throughout the evolution and decay of the IOD years with some underestimation.

Figure 7 shows the composite evolution of anomalous subsurface current, zonal wind stress (averaged over 60°E–90°E, 2°S–2°N) and equatorial subsurface pressure difference (west minus east). The initial trigger is found in the wind stress, which occurs in May. During strong


Fig. 6 Composite evolution of zonal windstress anomalies (*shaded*) and surface (15 m depth) zonal current anomalies from model (*contours*) during **a** strong IOD years and **b** weak IOD years. Composite evolution of sea surface salinity anomalies (*shaded*) and subsur-face zonal current anomalies (*contours*) from model during **c** strong IOD years and **d** weak IOD years. All the fields are averaged over 1.5°S–1.5°N
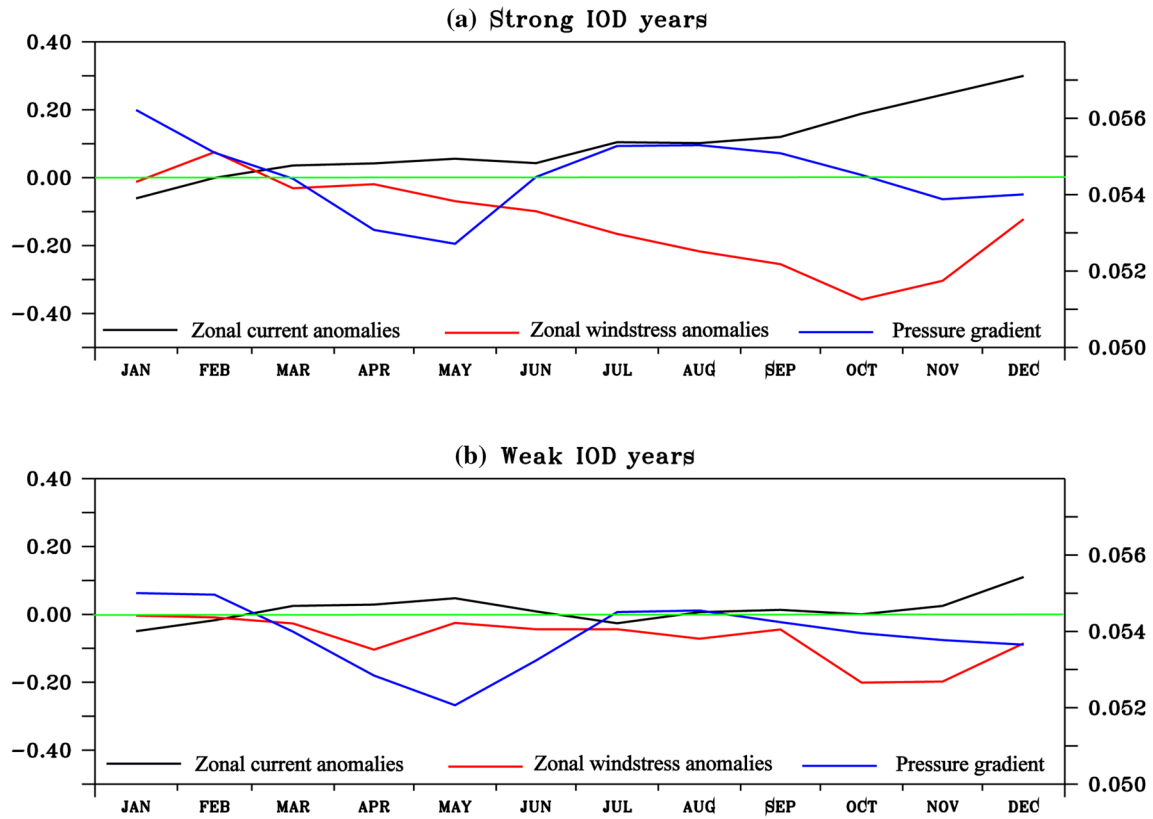
Fig. 7 Composite evolution of subsurface zonal current anomalies (*black*), zonal wind stress anomalies (*red*) averaged over 60°E–90°E, 2°S–2°N and normalized equatorial subsurface pressure gradient force (*blue*; subsurface pressure difference: western EIO minus eastern EIO) during **a** strong IOD years and **b** weak IOD years
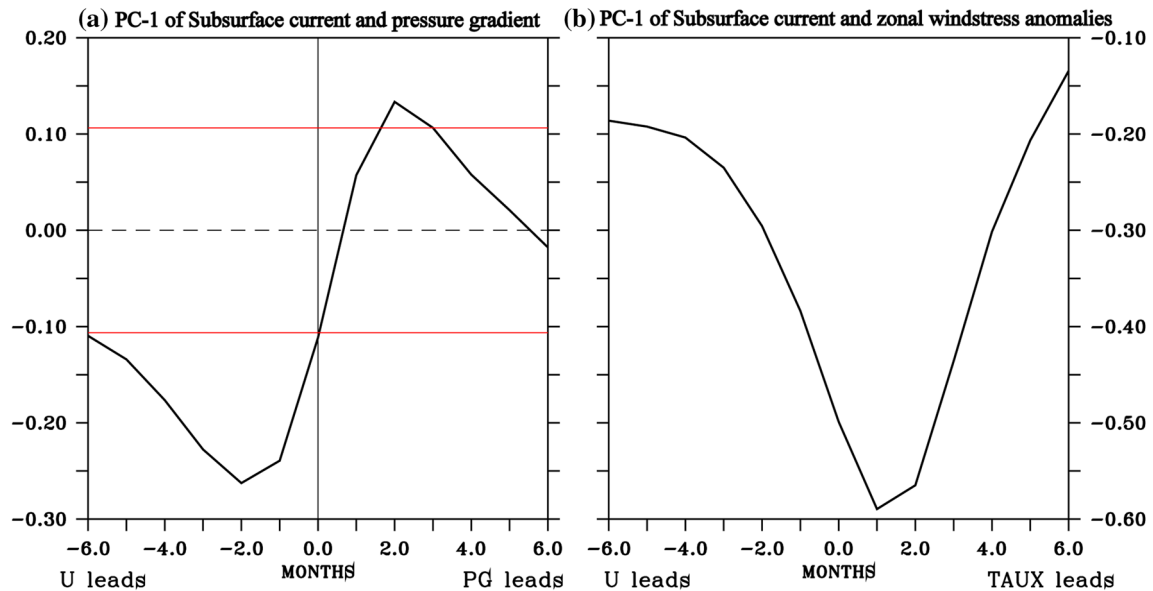

Fig. 8 Lead lag correlation between PC1 of anomalous **a** subsurface pressure gradient and subsurface current and **b** zonal winds and subsurface current

years, the anomalous winds are easterly and evolve strongly throughout the year. As a response to the anomalous winds, the surface zonal current anomaly turns westward and concurrently the subsurface current anomaly turns eastward during strong IOD years. Though the initial trigger is by winds, both easterly anomalies and anomalous pressure gradient force support the ESC, therefore it is mandatory to examine the evolution of anomalous pressure gradient as well. The pressure gradient force term has been computed as the difference in subsurface pressure between western EIO (50°E–70°E, 1.5°S–1.5°N) and eastern EIO (80°E–100°E, 1.5°S–1.5°N). This difference in pressure is effectively a normalized pressure gradient force. The annual cycle of eastward equatorial subsurface pressure

gradient force weakens consistently from January and is at its weakest in May with second minima during fall season. On the other hand the eastward pressure gradient force is anomalously high during strong IOD years especially during June–September (Fig. 7). The subsurface pressure gradient force is towards east during strong IOD years (June–September) and the ESC evolves consistently with it. In contrast, the subsurface pressure gradient remains weak throughout the year during weak IOD years. In weak IOD years, the ESC is weak even during the peak phase of IOD. The first sign of an anomalous subsurface current is evident in March during strong IOD years in the eastern region. This anomalous eastward flow extends to the surface in April during strong years, while it remains in the
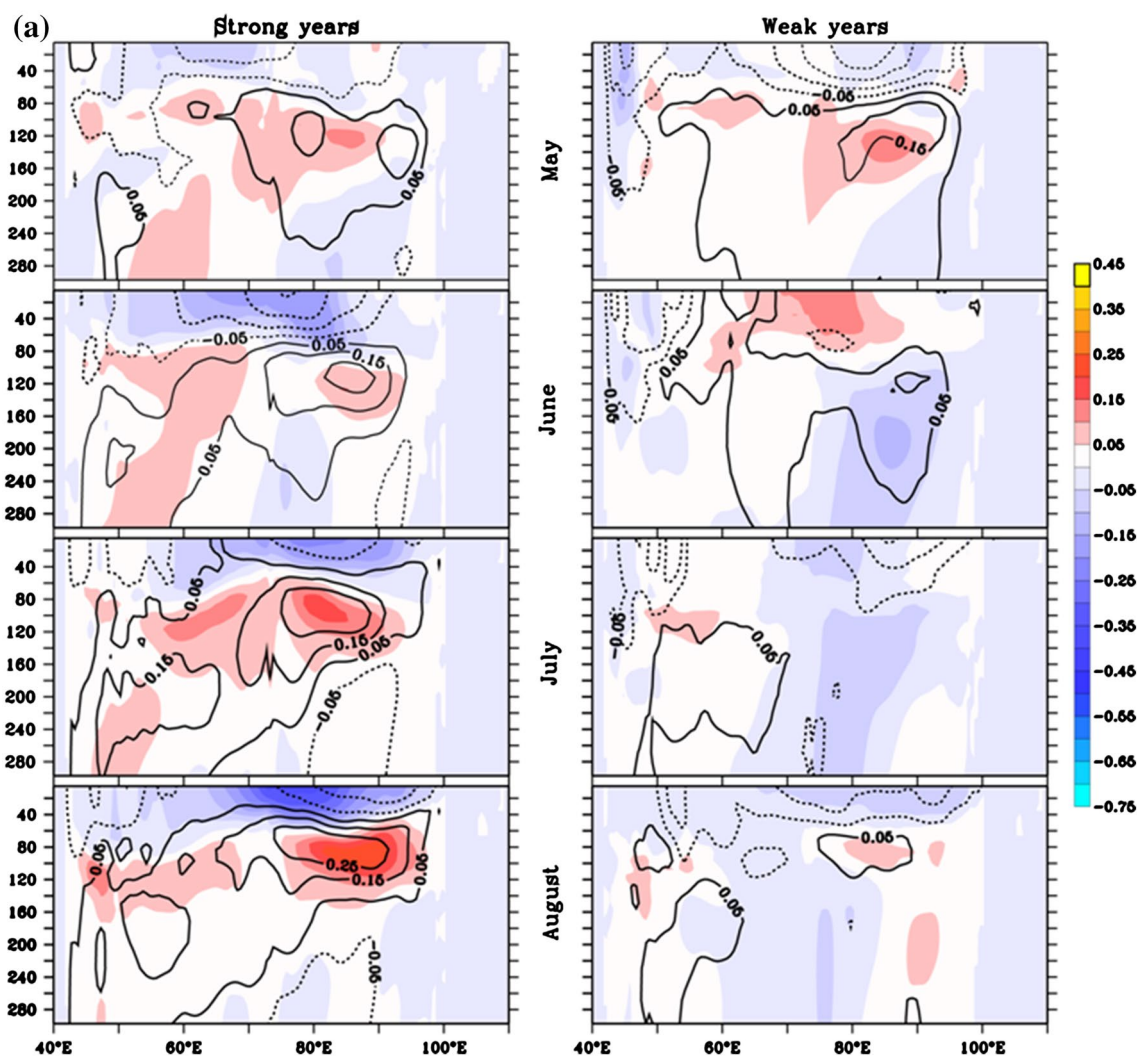
Fig. 9 **a** Depth longitude sections of subsurface zonal current anomaly composites (m/s) averaged over 1.5°S–1.5°N from May to August for strong IOD years (*left panels*) and for weak IOD years (*right panels*) from model (*shaded*) and SODA (*contours*). **b** Depth longitude

sections of subsurface zonal current anomaly composites (m/s) averaged over 1.5°S–1.5°N from September to December for strong IOD years (*left panels*) and for weak IOD years (*right panels*) from model (*shaded*) and SODA (*contours*)
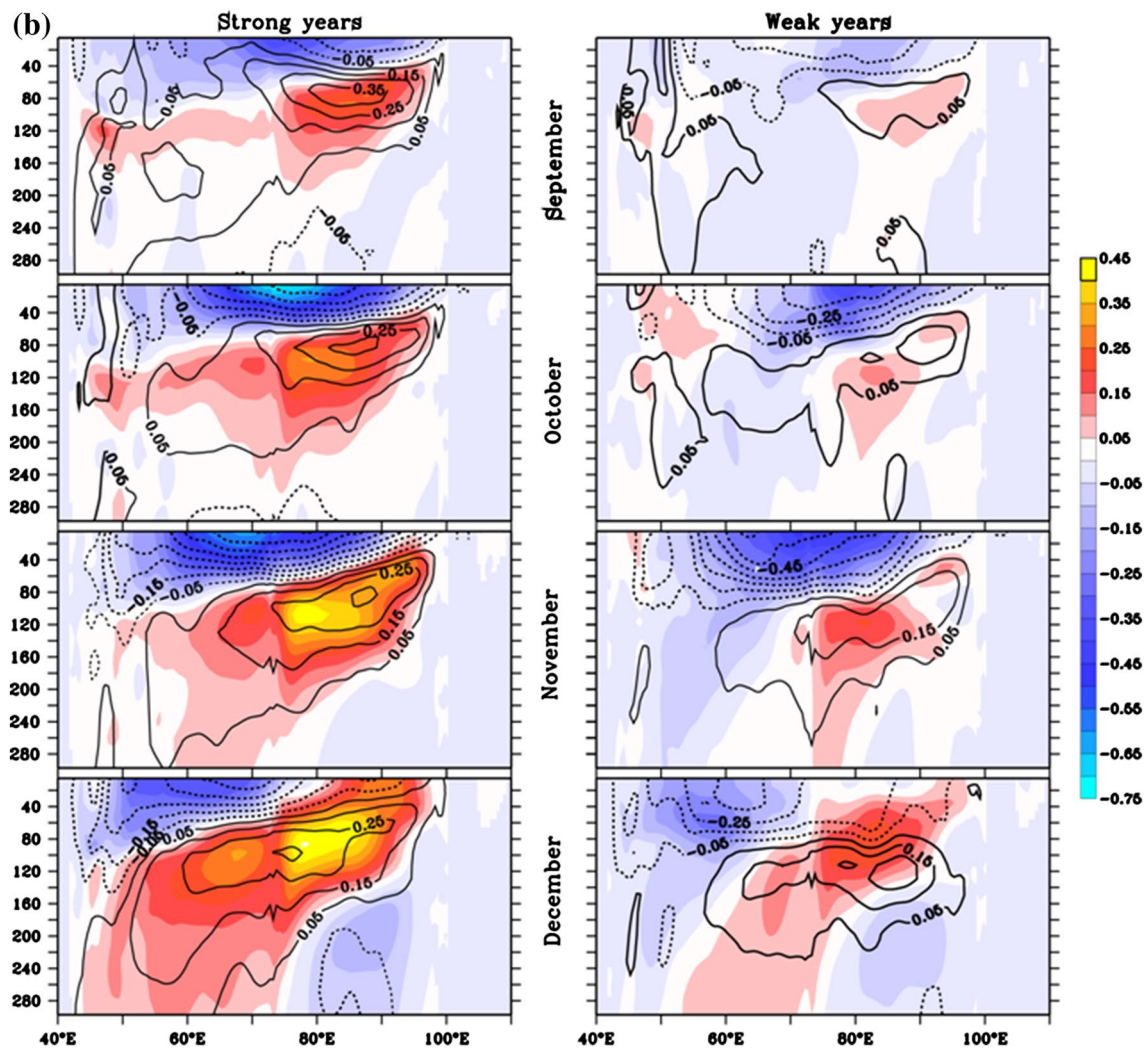
Fig. 9 (continued)

subsurface region during weak years. From this it is evident that in the extreme eastern region, the surface manifestation of an anomalous flow is evident in the month of April in the case of strong IOD years.

PC-1 of zonal subsurface current shows maximum correlation with subsurface pressure gradient at a lag of 2 months (Fig. 8a) and with anomalous equatorial zonal wind stress at 1 month lag (Fig. 8b). It also suggests that the changes in the subsurface currents are partially responsible for changes in the subsurface pressure gradient. Figures 5 and 8b consistently show that the surface equatorial winds are the main trigger for the anomalous evolution of the subsurface pressure gradient and equatorial subsurface current.

Composite evolution of the vertical structure of zonal currents during the strong and weak IOD years from May onwards is shown in Fig. 9. May undercurrent is similar in both cases while significant difference is seen in the surface

flow of June composites. Surface current anomalies show first significant differences in June with westward (eastward) current throughout the basin during strong (weak) IOD years. The subsurface current is anomalously eastward during strong IOD years, while the anomalies are insignificant during weak IOD years. From June onwards, the equatorial undercurrent evolves consistently during strong IOD years, and reaches its maximum amplitude during fall and remains strong up to the end of the year. The anomalous ESC strengthens consistently through the months of July and August during strong IOD years whereas the flow remains weakly westward throughout the basin during weak IOD years. From September onwards, the anomalous ESC extends to the extreme ends of eastern EIO with a strongly westward surface flow driven by anomalous easterly surface winds. During weak IOD years, the undercurrent is far weaker compared to the undercurrent observed during strong IOD years. Since ESC is an important component of
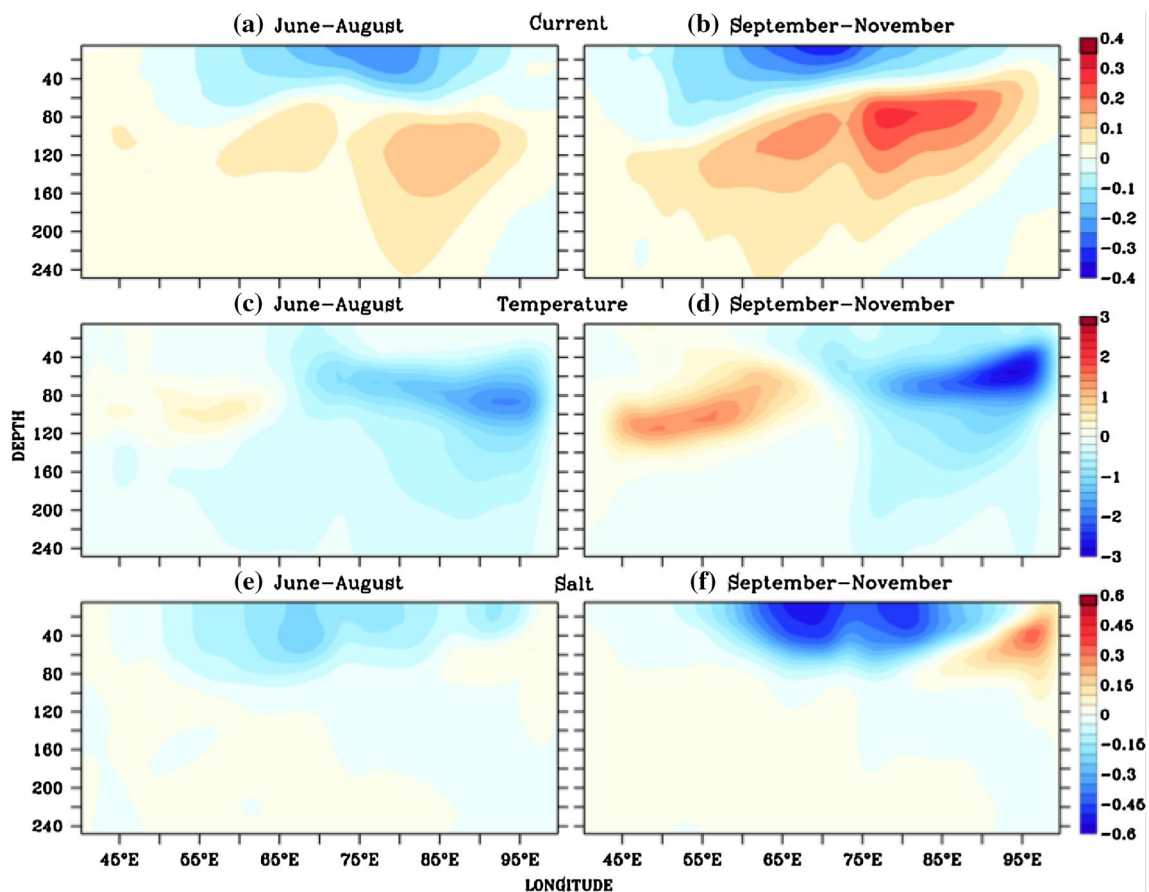
Fig. 10 Depth longitude difference of zonal current anomaly composites (m/s) (*top panels*), temperature anomaly composites (*middle panels*) and salinity anomaly composites (*bottom panels*) between strong and weak IOD years averaged over 1.5°S–1.5°N during June to August (**a, c, e**) and September to December (**b, d, f**) from model

upwelling process in the eastern EIO during IOD years, the analysis suggests that the subsurface current evolution may play a significant role in amplifying the upwelling in the eastern EIO region. The occurrence of such a strong anomalous eastward undercurrent during summer of strong IOD years may partly be explained by the equatorial eastward pressure gradient force (Fig. 7).

Figure 10 shows the depth-longitude plot of differences in anomalous currents, temperature and salinity between strong and weak IOD years averaged over 1.5°S–1.5°N. Concurrent with the zonal current anomalies (Fig. 10a, b), the seasonal composite of subsurface temperature anomaly shows stronger upwelling during the summer of the developing phase of strong IOD (Fig. 10a). Negative subsurface temperature anomalies are strongest in the peak phase of strong IOD. Along with the eastern EIO cooling, the strong IOD years also show subsurface warming in western EIO, which creates a strong zonal subsurface pressure gradient in which an eastward ESC may develop. Consistent with the EOF of ESC (Fig. 5a) and Fig. 10b (a peak each in the region west and east of 75°E), the surface salinity reveals

two maxima one in the west and the other in the east of 75°E. This further strengthens the possibility of EUC on air-sea coupling during strong IOD years. It has been shown that the subsurface current variability is strongly driven by IOD. However, the oceanic response to IOD forcing or thermocline-SST coupling is strongly dependent on whether the IOD is strong or weak (Deshpande et al. 2014).

5 Summary and discussion

The vertical structure and subsurface current variability are studied using a high resolution OGCM and reanalysis products. The vertical extent of Wyrtki jets is up to 80 m in both spring and fall beyond which the current weakens rapidly and reverses in the pycnocline. Eastward equatorial subsurface current (ESC) is well defined in the months of February and March at depths of σ-23 to σ-25 isopycnals, which is consistent with previous studies (e.g. Schott and McCreary 2001; Schott et al. 2009; Chen et al. 2015). EUC shows strong variability during summer

and fall seasons. The variability in ESC is found to be mainly dominated by IOD forcing, while Pacific forcing has weaker impact. PC-1 of ESC shows a significant correlation with DMI whereas both PC-1 and PC-2 have a weaker correlation with Niño 3.4 index. This suggests that the dominant mode of variability in the subsurface currents is mainly driven by IOD forcing, which affects both surface current and the subsurface pressure gradient and which may also change through variations in its internal dynamics. Detailed analysis of PC-1 of subsurface current reveals that although the primary variability is associated with IOD, the response of the subsurface currents is not same during all IOD years. Based on the criteria developed by Deshpande et al. (2014), the evolution of subsurface currents was further studied based on strong and weak IOD years. The eastward undercurrent during strong IOD years raises the thermocline in the east EIO and support upwelling throughout the evolution of IOD. During weak years, the undercurrent is evident only in the peak phase of IOD and D20 anomalies remain weaker.

Deshpande et al. (2014) have shown that strengthened monsoon over the Indian subcontinent (especially over the monsoon trough region) is evident only during strong IOD years. The weak IOD years show less impact on summer monsoon rainfall. The present study concludes that a well defined dynamic coupling between surface and subsurface is seen only during strong IOD years, which is supported by ESC response in the EIO, where the anomalous eastward undercurrent evolves coherently since June and continues to remain strongly eastward till the peak phase of strong IOD years. In contrast, the lack of subsurface current evolution may be one of the reasons for the inconsistent thermocline-SST coupling during the weak IOD years. The equatorial wave dynamics may be the potential factor for the differences in the ocean response. Nyadjro and McPhaden (2014) observed that the IOD events could influence the processes in the year following the events due to equatorial wave dynamics. Gnanaseelan et al. (2008) and Gnanaseelan and Vaid (2010) also reported biennial equatorially trapped Rossby waves lingering during the IOD years, which may be inducing the differences in the processes during strong and weak IOD years. The EIO thermocline response is a significant factor governing the evolution of IOD events and their impact on regional climate. Thus the importance of equatorial dynamics, particularly subsurface current variability and its impact on the evolution of dominant air-sea coupled modes has been highlighted in this study.

References

Carton JA, Giese BS (2008) A reanalysis of ocean climate using simple ocean data assimilation (SODA). Mon Weather Rev 136:2999–3017

Chen G, Han W, Li Y, Wang D, McPhaden MJ (2015) Seasonal-to-interannual time scale dynamics of the equatorial undercurrent in the Indian ocean. J Phys Oceanogr 45:1532–1553. doi:10.1175/JPO-D-14-0225.1

Chowdary JS, Gnanaseelan C, Xie SP (2009) Westward propagation of barrier layer formation in the 2006–07 Rossby wave event over the tropical southwest Indian ocean. Geophys Res Lett 36(4):L04607. doi:10.1029/2008GL036642

Deshpande A, Chowdary JS, Gnanaseelan C (2014) Role of thermocline–SST coupling in the evolution of IOD events and their regional impacts. Clim Dyn 43:163–174. doi:10.1007/s00382-013-1879-5

Gadgil S, Vinayachandran PN, Francis A, Gadgil S (2004) Extremes of the Indian summer monsoon rainfall, ENSO and equatorial Indian Ocean oscillation. Geophys Res Lett 31:L12213. 10.1029/2004GL019733

Gnanaseelan C, Vaid BH (2010) Interannual variability in the Biannual Rossby waves in the tropical Indian ocean and its relation to Indian ocean dipole and El Niño forcing. Ocean Dyn 60(1):27–40

Gnanaseelan C, Vaid BH, Polito PS (2008) Impact of biannual Rossby waves on the Indian ocean dipole. IEEE Geosci Remote Sens Lett 5(3):427–429

Gnanaseelan C, Deshpande A, McPhaden MJ (2012) Impact of Indian ocean dipole and El niño/southern oscillation forcing on the Wyrtki jets. J Geophys Res 117:C08005. doi:10.1029/2012JC007918

Griffies SM, Biastoch A, Böning C et al (2009) Coordinated ocean-ice reference experiments (COREs). Ocean Model 26(1–2):1–46. doi:10.1016/j.ocemod.2008.08.007

Iskandar I, Masumoto Y, Mizuno K (2009) Subsurface equatorial zonal current in the eastern Indian ocean. J Geophys Res 114:C06005. doi:10.1029/2008JC005188

Izumo T (2005) The equatorial undercurrent, meridional overturning circulation, and their roles in mass and heat exchanges during El Niño events in the tropical Pacific ocean. Ocean Dyn 55:110–123. DOI:10.1007/s10236-005-0115-1

McPhaden MJ, Meyers G, Ando K, Masumoto Y, Murty VSN, Ravichandran M, Syamsudin F, Vialard J, Yu L, Yu W (2009) RAMA: the research moored array for African–Asian–Australian monsoon analysis and prediction. Bull Amer Meteor Soc 90:459–480. doi:10.1175/2008BAMS2608.1

Nyadjro E, McPhaden MJ (2014) Variability of zonal currents in the eastern equatorial Indian ocean on seasonal to interannual time scales. J Geophys Res 119:7969–7986. doi:10.1002/2014JC010380

Rahul S, Gnanaseelan C (2016) Can large scale surface circulation changes modulate the sea surface warming pattern in the Tropical Indian ocean? Clim Dyn 46:3617–3632. doi:10.1007/s00382-015-2790-z

Reppin J, Schott FA, Fischer J, Quadfasel D (1999) Equatorial currents and transports in the upper central Indian ocean: annual cycle and interannual variability. J Geophys Res 104:15,495–15,514. doi:10.1029/1999JC900093

Saji NH, Goswami BN, Vinayachandran PN, Yamagata T (1999) A dipole mode in the tropical Indian ocean. Nature 401:360–363

Sayantani O, Gnanaseelan C (2015) Tropical Indian Ocean subsurface temperature variability and the forcing mechanisms. Clim Dyn 44:2447–2462. doi:10.1007/s00382-014-2379-y

Schott F, McCreary JP (2001) The monsoon circulation of the Indian ocean. Prog Oceanogr 51:1–123

Schott F, Xie SP, McCreary JP (2009) Indian ocean circulation and climate variability. Rev Geophys 47:1–46. doi:10.1029/2007RG000245.1

Swapna P, Krishnan R (2008) Equatorial undercurrents associated with Indian ocean dipole events during contrasting summer monsoons. Geophys Res Lett 35:L14S04. doi:10.1029/2008GL033430

Thompson B, Gnanaseelan C, Salvekar PS (2006) Variability in the Indian ocean circulation and salinity and its impact on SST anomalies during dipole events. J Marine Res 64:853–880. doi:10.1357/002224006779698350

Vinayachandran PN, Saji NH, Yamagata T (1999) Response of the equatorial Indian Ocean to an unusual wind event during 1994. Geophys Res Lett 26(11):1613–1616. doi:10.1029/1999GL900179

Webster PJ, Moore AW, Loschnigg JP, Leben RR (1999) Coupled ocean-atmosphere dynamics in the Indian ocean during 1997–1998. Nature 401:356–360

Wyrtki K (1973) An equatorial jet in the Indian ocean. Science 181:262–264

Xie SP, Annamalai H, Schott FA, McCreary JP (2002) Structure and mechanisms of South Indian ocean climate variability. J Clim 15:864–878

Zhang D, McPhaden MJ, Lee T (2014) Observed interannual variability of zonal currents in the equatorial Indian ocean thermocline and their relation to Indian ocean dipole. Geophys Res Lett 41:7933–7941. doi:10.1002/2014GL061449